

# Accepted Manuscript

Transverse permeability of dry fiber preforms manufactured by automated fiber placement

A.R. Aziz, M.A. Ali, X. Zeng, R. Umer, P. Schubel, W.J. Cantwell



PII: S0266-3538(17)31610-X

DOI: [10.1016/j.compscitech.2017.09.011](https://doi.org/10.1016/j.compscitech.2017.09.011)

Reference: CSTE 6900

To appear in: *Composites Science and Technology*

Received Date: 4 July 2017

Revised Date: 22 August 2017

Accepted Date: 9 September 2017

Please cite this article as: Aziz AR, Ali MA, Zeng X, Umer R, Schubel P, Cantwell WJ, Transverse permeability of dry fiber preforms manufactured by automated fiber placement, *Composites Science and Technology* (2017), doi: 10.1016/j.compscitech.2017.09.011.

This is a PDF file of an unedited manuscript that has been accepted for publication. As a service to our customers we are providing this early version of the manuscript. The manuscript will undergo copyediting, typesetting, and review of the resulting proof before it is published in its final form. Please note that during the production process errors may be discovered which could affect the content, and all legal disclaimers that apply to the journal pertain.

## Transverse permeability of dry fiber preforms manufactured by automated fiber placement

AR Aziz<sup>1</sup>, MA Ali<sup>1</sup>, X Zeng<sup>2</sup>, R Umer<sup>\*1,2</sup>, P Schubel<sup>2</sup>, WJ Cantwell<sup>1</sup>

<sup>1</sup>Department of Aerospace Engineering, Khalifa University of Science and Technology, Abu Dhabi, UAE.

<sup>2</sup> Centre for Future Materials, University of Southern Queensland, Toowoomba, QLD, 4390, Australia

\*Corresponding Author Email: rehan.umer@usq.edu.au

Ph: +61 7 4631 5516

### Abstract

This work presents a correlation between the transverse permeability of a preform and the process variability of the automated dry fiber placement manufacturing technique. In this study, an experimental and numerical analysis of the dry tape preform, with a focus on its through-thickness permeability, has been undertaken. Geometric models, containing flow channels of two different width dry tape carbon preforms, have been created in the TexGen modeller. A Computational fluid dynamics (CFD) simulation has been undertaken to obtain the predicted through-thickness-permeability of the dry tape preform. A parametric study on the effect of different dry tape gap sizes on the permeability of the preform is presented. An in-situ compaction study, carried out in an X-CT machine, revealed that the gap sizes were irregular throughout the manufactured preforms. In addition, an experimental investigation of the through-thickness permeability, which is based on a saturated flow condition at a thickness corresponding to full vacuum pressure, is also presented. The permeability prediction based on the X-CT re-constructed geometric model has been validated using the experimental data. A further parametric study has revealed that the process variability in automated dry fibre placement influences the through-thickness permeability by a factor of upto 5.

**Key Words:** Modeling; Automated Fiber Placement; Layered structures; Resin flow

## 1.0 Introduction

Liquid composite molding (LCM) includes a number of composite manufacturing techniques [1-5], all of which require a vital, yet time-consuming preforming step. In recent past, preforming has been achieved by 2D/3D weaving, fabric draping, and stitching. These procedures require high-end textile processing capabilities, which are expensive, time consuming, and labour-intensive. The automated fiber placement (AFP) technique [6-8], is an innovative way of overcoming many preforming problems. The process utilizes a robotic arm, which deposits dry fibers onto a complex mold, potentially overcoming any fabric structure variability and variations in local fiber volume fraction, while draping in complex or tight corners. This technology has been successfully implemented on the wing box of recent MS-21 airplane and C frames of upcoming aircraft fuselages [9, 10]. Recently, a number of commercial dry fiber tape reinforcements have been developed, examples being unidirectional carbon fiber tape from Solvay (PRISM TX1100 UD-dry tape) and Hexcel (HiTape).

The dry fiber tapes offer cost and weight advantages over traditional thermoset prepreg systems, by keeping the raw material and, finished preform at room temperature with unlimited shelf life [7]. The modern dry fiber tape manufacturers use binding agents for good tack to the mold, and subsequent layers when heated, and a permeable veil between the fibers for better resin impregnation. In order to allow high-speed production, a powerful heating source such as a laser, has to be incorporated to activate the binder. Furthermore, the response time of the heating device needs to be as rapid as possible, to avoid any ply spring-back [11]. It is well known that, fiber reinforcements exhibit viscoelastic compaction response [12-14]. Tape compression through AFP rollers also play a significant role in determining the final part quality, given that the first ply will be compressed several times, while the last ply will be compressed only once and the resulting preform may be non-homogeneous in the through-thickness direction.

Permeability is the ease with which a fluid can flow through a reinforcement and is primarily a function of the reinforcement architecture and its fiber volume fraction. The fibrous reinforcements are dual-scale porous media and generally exhibit different permeabilities in different material directions, i.e. the values of the two in-plane permeabilities,  $K_{11}$  and  $K_{22}$ , and the through-thickness permeability,  $K_{33}$ , are different. Although determining the complete permeability tensor is important, the through-thickness

permeability is crucial in controlling the final thickness of the cured product. With increased preform thickness, the influence of through-thickness permeability on LCM processing of composites becomes increasingly significant [15-17]. When resin injection is facilitated in transverse direction, by using a distribution medium, such as in the Vacuum Assisted Resin Transfer Molding (VARTM),  $K_{33}$  becomes the dominant parameter. Experimentally, the through-thickness permeability is determined in a saturated flow regime, as compared to transient flow for the in-plane permeability. This is primarily because of difficulties in monitoring the flow advancement through the thickness of the preform [18].

Recent work on permeability of dry tape preforms has focused on the experimental analysis by varying gap sizes, binder amounts, layup sequence, and tufting of preforms, in order to enhance the permeability [19, 20]. However, no study has considered a detailed experimental and computational modelling approach for permeability predictions of AFP dry tape preforms. The main objective of this research is to correlate the variability of the automated dry fibre placement process, and the through-thickness permeability of manufactured dry tape preforms. A detailed finite element analysis using a geometric model of the preform, in-situ compaction in an X-ray computerized tomographic (X-CT) machine, parametric studies on the gap sizes for efficient resin flow, permeability computations based on the re-constructed geometry of the preforms after scanning, and finally, experimental validation through permeability experiments is developed. The following summarizes the step-by-step approach,

- i. Two different dry tape based preforms, with a target 0.2 mm gap size between the tapes, were manufactured using an automated fiber placement machine.
- ii. Geometric models of ideal dry tape preforms were created in the TexGen modeller, with the focus on determination of their through-thickness permeability.
- iii. A parametric study on the effect of varying the gap size on the permeability was conducted.
- iv. A detailed X-CT analysis of the dry tape preforms compacted inside the X-CT machine was undertaken, highlighting the variability in the gaps produced by the AFP machine.
- v. The scanned structures were re-constructed in TexGen, modelled and the through-thickness permeability was compared with the experimental and numerical results.

## 2.0 Materials

The dry fiber tapes (PRISM TX1100) used in this study were supplied by Solvay, Wrexham, UK. The dry tape uses a proprietary veil and binder technology which is incorporated to improve resin flow and tack. The preforms were manufactured using the AFP manufacturing process. Here, a robot with a 6 kW laser mounted on the Coriolis end-effector, was used to place the fibers on a flat mold. The heat generated by the laser was sufficient to activate the binder that ensured bonding of adjacent tows. The panels were manufactured after adjusting the tow gap to facilitate resin flow. Preform A, having 6.35 mm, and Preform B having 12.7 mm wide tapes with targeted inter-tape gaps of 0.2 mm were investigated, see Figure 1a. Each preform consists of 24 layers with a stacking sequence of  $[+45/0/-45/90]_{3s}$ , giving an overall thickness of 5.15 mm. For the fibers, unidirectional Tenax IMS65 carbon fibers with a filament diameter of 5  $\mu\text{m}$  were used.

## 3.0 Model Development

In this study, 3D geometrical models of the carbon fiber dry tape preform were created in the TexGen modeller using a graphical user interface (GUI). Two geometric definitions are considered here, the ideal tape placement with uniform gaps of 0.2 mm, and the realistic tape placement with varying gap sizes. For modelling the realistic tape placement, the width, height and relative location of individual tow gaps were measured from the X-CT scan data using the ImageJ software. The TexGen model was then constructed from the measured parameters. The TexGen model was meshed and exported as an input file for the flow analysis in ANSYS-CFX. The workflow between TexGen and ANSYS is detailed in the online tutorial [21]. For modelling the ideal tape placement, the dry tape geometries were modelled as per the manufacturer's data, the veil and the binder was ignored in this model for simplicity. For the dry tape preform studied here, the tapes were assumed to be impervious to flow given that the permeability, which can be approximated by the tow volume fraction using Gebart's model [22], is typically two orders of magnitude smaller than the macroscopic permeability [2, 3]. Hence, steady-state flow through the channels was modelled, given that the fluid will travel more rapidly through the gaps between the tapes. This assumption greatly reduces the computational cost of the

flow simulation. Figure 1b shows a dry tape preform model, created by stacking layers of quasi-isotropic unidirectional tapes. In order to discretise the preform into a computational mesh, appropriate numbers and types of elements were defined in the x, y and z directions.

Computational fluid dynamics (CFD) simulations were carried out using the commercial code ANSYS/CFX for the permeability analysis of the generated matrix mesh imported from the ANSYS/finite element modeller. In the CFX-Pre processor, the boundary conditions are defined. The preform with a stacking sequence of  $[+45/0/-45/90]_{3s}$  has no in-plane periodicity in a Cartesian coordinate system. The experimental sample size was 100 mm in diameter, a model of similar size was not used instead, the numerical model was maximised to the size 50 mm x 50 mm. Larger size models produced similar results but at the expense of high computational time and costs. Two types of boundary conditions, symmetric and a non-slip wall for the side faces were initially tested. The permeability predictions resulted in a difference of approximately 0.2%. The current model was not sensitive to the boundary conditions of the side faces, hence, the default boundary condition of a non-slip wall was applied on the side faces for all subsequent analyses. The top face was applied with a uniform pressure of 1 Pa, while the bottom face was applied with a uniform pressure of 0 Pa. The pressure drop  $\Delta p$  therefore equates to 1 Pa, which induces a mass flow in the through-thickness direction. Figure 2(a) shows the boundary conditions for the dry tape used in the ANSYS model for through-thickness permeability predictions. The numerical study conducts a laminar flow simulation, with a pressure length of 4.8 mm, i.e. the thickness of the compressed preform under vacuum pressure. The non-slip wall boundary conditions were specified at the four side surfaces of the fluid domain, as well as between the tapes and the fluid interfaces for the through-thickness flow simulation. Figure 2(b) and 2(c) show top surface views of the ANSYS models for Preform A and Preform B, respectively.

Once the simulation parameters were defined in the CFX-Pre processor, the CFX-Solver was used to run and solve all of the flow field variables for flow simulation based on the discretisation of the Navier-Stokes continuity and momentum equations [23]. ANSYS CFD-Post was used for post-processing the simulation results and to obtain the necessary information for the permeability calculations. During the post-processing stage, the flow paths are visualised and volume averaged mass flow-rate is obtained. With

the applied pressure gradient and known geometry, the permeability through the gaps between the tapes is calculated according to Darcy's law [22]. To obtain a reasonable balance between accuracy and computation time, the accuracy of the CFX calculations to the mesh size was assessed, based on convergence of the predicted through-thickness permeability of the AFP tape. To summarize, the processes involved in modelling the through-thickness permeability is illustrated in the form of a flowchart in Figure 3. This study also involved a numerical parametric study to optimize the through-thickness permeability of Preform B in a 50 mm x 50 mm model. To explore the effect of varying the gap size, values of 0.1, 0.3 and 0.4 mm were considered. A further investigation was carried out by alternating the reference 0.2 mm gap with 0.1, 0.3 and 0.4 mm gaps. The gap height of 0.2 mm was maintained constant throughout.

## 4.0 Experimental

### 4.1 Microscopy and X-CT Analysis

Initially, the preform morphology was investigated by examining tape cross-sections under optical microscopy. The tape fiber volume fraction,  $V_f$  was estimated using ImageJ software [24],

$$V_f = \frac{A_f}{A_t} \cdot N_f \quad (1)$$

where  $A_f$  is the cross sectional area of a single fiber in the image,  $A_t$  is the total area of the tape image under investigation, and  $N_f$  is the total number of fibers in the image. Five measurements were taken at different locations for each tape to achieve more accurate results.

The X-CT images were obtained using a GE<sup>®</sup> Phoenix Nanotom device to study the microstructure of the preform, specifically the gaps between the tapes. A 40 mm diameter compaction fixture was installed in the X-CT machine with a load cell capacity of 5 kN. The 40 mm diameter preform samples were placed between the two platens, and a compaction force equivalent to full vacuum pressure was applied at the crosshead speed of 0.5 mm/min. After one hour, when complete stress relaxation of the preform was achieved, scanning was undertaken at voxel size of 25  $\mu\text{m}$ . The X-CT experimental set-up and an illustration of image acquisition are presented in Figure 4 (a,b). The commercial packages, VGStudio Max

and GeoDict, were used for data processing, evaluation and the gap analysis. A bimodal threshold was applied to the voxel intensity histogram to segment the pores and the preform [24, 25].

## 4.2 Through-thickness Permeability Experiments

Following the microstructural analysis, the through-thickness permeability was measured using an existing saturated unidirectional flow measurement device, as shown in Figure 5(a,b). The device was housed within a 300 kN MTS testing frame, allowing for accurate control of the sample thickness, and the potential for simultaneous compressibility and permeability measurements. In the 150 mm diameter cylindrical fixture, the through-thickness flow area had a diameter of 100 mm, the flow direction is from the bottom inlet to the top flow outlet, passing through the sample held between the plates with holes as shown in the schematic in Figure 5(b). The sample thickness (4.8 mm corresponding to 58.5%  $V_f$ ) was ensured using a linear variable displacement transducer (LVDT) sensor, allowing for the calculation of actual  $V_f$  values. The through-thickness permeability was computed from the measured flow rate using Darcy's law;

$$K_{33} = \frac{Qh\mu}{A \cdot \Delta P} \quad (2)$$

where  $Q$  is the volumetric flow rate through the sample,  $h$  is the imposed cavity thickness,  $\mu$  is the hydraulic oil (test fluid) viscosity, 0.078 Pa.s,  $A$  is the cross sectional area, and  $\Delta P$  is the applied pressure difference. Due to limited availability of the materials, three experiments were conducted for each of the permeability characterization experiments to get an average value.

## 5.0 Results and Discussion

### 5.1 CFD Prediction on the Effect of Gaps on the Permeability

The FE flow simulations were performed on Preform A and Preform B, as shown in Figures 2 (b,c). The flow velocity values were obtained from the CFX post-processor and the permeability was calculated by applying Darcy's law. It is necessary to do a mesh sensitivity analysis before validation of the permeability value, since the number of meshed elements through the gap width and thickness will effect the accuracy of final results. To assess the sensitivity of the permeability prediction, flow simulation on



Preform A was chosen for this study. The finite element model was meshed using eight different mesh sizes from 0.12 to 0.03 mm, with the number of nodes ranging from 128,000 to 2,473,000, as listed in Table 1.

Figure 6 summarizes the findings of this mesh sensitivity analysis, where the relationships between the number of nodes and the predicted permeability and CPU run time are shown. The figure shows that the predicted permeability decreases as the mesh is refined, tending towards a constant value when a very detailed mesh is employed. Closer examination of Figure 6 and Table 1 suggests that a model with  $650 \times 10^3$  nodes is sufficient with a 90% confidence level of the converged prediction. The resulting model, with an element size of 0.05 mm, was deemed to represent a suitable compromise between model accuracy and overall CPU time.

Table 2 presents the predicted CFD results for the through-thickness permeability of Preform A and Preform B. The % gaps in the 3D design is based on the ratio of the volume of gaps to the total volume of the domain. The permeability in the through-thickness direction obtained from the CFD analyses of Preform A and Preform B were  $3.87 \times 10^{-13}$  and  $3.65 \times 10^{-14} \text{ m}^2$ , respectively. Clearly, the permeability of the preform based on the 12.7 mm wide tapes is approximately 90% lower than preforms based on 6.35 mm wide tapes. A higher flow channel density can be observed in Preform A compared to Preform B, as shown in Figures 2 (b,c). This visual observation suggests that the permeability is much higher in Preform A, which agrees with the computational permeability results.

Figure 7 and Table 3 present the calculated permeability values for different gap widths for the Preform B. The bar chart gives the predicted permeabilities of preforms with inter-tape gaps of 0.1, 0.2, 0.3 and 0.4 mm and compares these values to those of preforms with similar gaps that alternate between 0.2 mm spacings, for example, 0.1, 0.2, 0.1, 0.2 mm etc. An examination of the figure shows that the permeability increases rapidly as the width of the gap between the tapes is increased from 0.1 to 0.4 mm. For example, the permeability for the smallest gap size based preforms is  $9.61 \times 10^{-15} \text{ m}^2$  whereas that for its 0.4 mm counterpart is  $1.34 \times 10^{-13} \text{ m}^2$ , i.e. over one order of magnitude greater. As expected, alternating the gap size by introducing 0.2 mm wide spaces between these gaps serves to increase the permeability of the 0.1 mm gap based preform and decrease those associated with the 0.3 and 0.4 mm systems. It is interesting to note that the values for the alternating 0.2/0.4 mm tape gaps in the preform with an average

gap size of 0.3 mm exhibits a slightly lower permeability than the standard 0.3 mm gap based preform, in spite of the fact that the % gap is the same in both cases.

## 5.2 Microscopy and X-CT Analysis

The cured preforms were examined under an optical microscope to physically study their microstructure. Figure 8a illustrates a typical cross-section micrograph image for Preform A following resin infusion. It can be observed that the unidirectional fibers form an almost circular shape for the 90° (out of plane) tape and close to an oval shape for the 45° angle. A gap due to surface veil and binder can be clearly identified as a darker region of approximately 20µm size in between the layers. Figure 8b shows a cross-section image consisting of the 90° fibers analysed using the ImageJ software. The fibers can be seen to be scattered, with the more compact fibers being packed in a hexagonal arrangement. Measurements yielded an average fiber diameter of 5 µm. By calculating the area of a focus part of the tape, the area of each fiber and the number of fibers, the average fiber volume fraction of the entire individual tape was estimated to be 0.74 in a 0.585 fiber volume fraction preform.

Microscopic inspection of Preform A and Preform B revealed that there were some irregularities in the gap sizes. Hence, a pore size distribution study was conducted on the preforms via a X-CT scan. The specimen has a thickness of 4.8 mm under full vacuum, and the experimental data shown in Figure 9 were obtained by decreasing the thickness from the uncompressed value to 4.8 mm, and then maintaining the thickness at this value during the relaxation process. The first phase starts with a rapid increase in the elastic region with time. The stresses reached a peak of approximately 0.12 MPa for both Preform A and Preform B. An abrupt drop in stress occurred and the preforms continue to relax at a constant value with increasing time, until there is no further decrease. A detailed X-CT scan was performed on the preform when stress relaxation was not observed anymore.

The re-constructed images of the preforms taken from the X-CT machine were analyzed using the VGStudio MAX software. Figure 10 (a,c) shows typical 3D X-CT scan images with the total volume of tapes and gaps captured. These images were transferred to GeoDict software, where the software interprets the tapes as a solid section and pores as gaps. Figure 10(b,d) shows the gap analysis images for Preform A

and Preform B from GeoDict. A closer inspection of the Figure 10(d) image reveals that some gaps are noticeably wider than others. From these images, very fine isolated gaps can also be observed, highlighting the binder material region. From the gap distribution analysis, it was found that the measured % gap of Preform A and Preform B were approximately 1.5% and 3.5% respectively.

Figure 11 shows the X-CT image slices of the preforms at selected depths, corresponding to plies oriented at +45°, 0°, 90° and -45° to the reference direction. An examination of the figure indicates that the gaps in Preform A are typically smaller than the anticipated value of 0.2 mm. The average gap widths in the +45°, 0°, 90° and -45° layers were 0.14, 0.14, 0.15 and 0.15 mm, respectively. A number of large gaps are apparent in Preform B, with values as high as 1.0 mm in cases. In this case, the average values for the gap size in the +45°, 0°, 90° and -45° layers were 0.59, 0.58, 0.25 and 0.26 mm, respectively. However, note that for both preforms, some gaps are clearly visible while others are difficult to distinguish.

The experimental through-thickness permeability characteristics of the AFP preforms based on the two different tape widths are summarised in Table 2. The average permeability of Preform B is approximately twice that of Preform A, with the former being  $1.85 \times 10^{-13} \text{ m}^2$  and the latter  $8.31 \times 10^{-14} \text{ m}^2$ . It was noted that the permeability variation in Preform B was more evident than in Preform A, due to limited availability of the raw materials and preforms, only an average of 3 experiments is presented. The unpaired two-tail Student's t-test was performed to measure the statistical significance between the two groups of samples. The two-tailed p-value of 0.07 shows that, the difference is not quite statistically significant. The higher degree of variation in Preform B causes the p-value to be slightly higher than the conventional criteria of 0.05. The permeabilities derived from CFD (geometrical design based) simulations are compared with experimental data in Table 2. An examination of the table indicates that the CFD model for Preform A overestimates the average experimental data by over 4.7 times. This relatively large discrepancy is related to the idealised geometry that was employed in the CFD models, where the actual dimensions of the test sample were not considered. An examination of Preform A in the X-CT scan revealed that the % gap in this sample was approximately 2.1 times lower than that in the CFD models. In contrast, Table 2 shows that the CFD prediction for Preform B underestimates the experimental value of permeability by approximately 5.1 times. As before, this can be explained by the difference in the measured

and calculated % gaps, where the % gap in the X-CT scan being approximately 2.3 times greater than that in the CFD model.

### 5.3 Effect of Tape Placement Variability on the Permeability

The X-CT analysis showed the significant geometric difference between the idealized preform model and the actual preform. This geometric difference resulted in the fivefold deviation between the permeability prediction and the experimental data. This finding strongly suggests that more consistent control of tape placement process would be desirable, in order to achieve the target permeability. This section attempts to quantify the exact effect of tape placement variability on the measured permeability. The accurate assessment of permeability was obtained through the geometric modelling of preform variability. The X-CT scans provided the basis to re-construct the precise preform geometry. The gaps were individually quantified for each ply orientation, with the measurements of cross-sectional width, cross-sectional height, and distance of ply shift. Another information was on, whether gaps disappeared due to tape overlap, this being the case for Preform A shown in Figure 11. Following the approach described in Section 3.0, the geometric model was constructed in TexGen to accurately replicate the X-CT scan. Figure 12 presents a through-thickness view of the stacked gaps in Preform A and Preform B. The TexGen models were closely matched with the X-CT scan in terms of the gap dimensions and the gap connections. The TexGen model was meshed using a voxel element size of 0.05 mm. This element size was based on the mesh sensitivity study described in Section 5.1. The subsequent CFD analysis and permeability calculation followed the procedure described in Section 3.0.

Table 2 also lists the CFD predictions based on the re-constructed X-CT geometric models. For both preforms, the CFD models accurately predicted the average experimental values with the greatest error being approximately 10%. Permeability inherently exhibits a large standard deviation, due to reinforcement deformation and measurement procedures [26]. The 10% discrepancy associated with the numerical prediction is considered as the extremely good result. It has always been a challenging task to accurately predict permeability of reinforcements due to fabric architectural variability. With advanced geometric and stochastic modelling approaches, the numerical predictions have significantly progressed, bringing

predictions much closer to experimental values [27, 28]. In the present study, the CT scans provide exact fiber architecture and variations in gap sizes in the actual preform sample. Also, the AFP dry preforms have simple geometric features compared to a woven or non-crimp fabric. The CT scans and relatively simple fiber architecture allow accurate geometric representations in the numerical modelling to achieve permeability predictions as close to experimental values.

For Preform A, in comparison to the idealized model based on the material geometrical design (Figure 2b), the re-constructed geometric model differed in the gap width by 20% narrower in average. The number of gaps was 27% less in the re-constructed geometric model due to the large number of tape overlaps. Tape overlap occurred in all the ply orientations. Here, we define the Tape Overlap Rate as the number of missing gaps over the total number of gaps based on the material design, times 100%. The Preform A was more prone to in-plane misalignment, than Preform B due to its narrower width. Hence, the tape placement process caused greater levels of tape overlap in Preform A. The narrower gap and the tape overlap decreased the permeability to just 20% of the idealized material design. For Preform B, the re-constructed geometric model had the much wider gaps, on average 300% that of the idealized model. The robotic arm failed to achieve the 0.2 mm tape gap in Preform B. As a result, the realistic permeability was four times greater than the target permeability value obtained from the idealized design. The large gaps, measuring up to 1.5 mm in Preform B, would likely to become resin-rich regions in the finished composite part. The resin-rich regions would represent potential paths for crack propagation, leading to a compromised mechanical performance.

The validated re-constructed TexGen model was adapted to perform parametric studies on the tape placement variability. The Tape Overlap Rate was 27% in Preform A model. By adding the missing gaps in sequence to the ply orientations  $+45^\circ$ ,  $90^\circ$ ,  $-45^\circ$ , and  $0^\circ$ , the Tape Overlap Rate gradually decreased to 18%, 9% and 0%. Also, by removing the existing gaps from the validated TexGen model, the Tape Overlap Rate increased up to 41%. The adapted models were then analyzed using the CFD analysis. Figure 13 (a) presents the sensitivity of predicted permeability to the Tape Overlap Rate. The Permeability decreases linearly with the Tape Overlap Rate. Permeability reached zero when the Tape Overlap Rate exceeds 50% and the gap connectivity was eliminated. Through-thickness permeability is highly dependant on the

connectivity of gaps. Figure 13 (b) highlights the quantified effect of tape placement variability. Taking the idealized preform design as the baseline, the re-constructed model with varied gap sizes had the most significant impact, with a 60% decrease on the through-thickness permeability. Further, to combine the varied gap size and the Tape Overlap Rate (modelling the actual preform), the Tape Overlap Rate led to a further 18% decrease in permeability. The parametric studies suggests a consistent control of gap width is critical in the tape placement process to achieve the design target for permeability.

## 6.0 Conclusions

An innovative modelling and experimental approach has been successfully applied to correlate the through-thickness permeability and the process variability of the automated dry fibre placement process. A versatile numerical model has been created and validated using experimental permeability measurements. Realistic TexGen models re-constructed from the X-CT scan, resulted in accurate permeability predictions with  $\pm 10\%$  deviation from the experimental data. The X-CT analysis, coupled with the in-situ compaction loading, provided the accurate 3D data of preform deformation. Supported by the accurate 3D geometric scan data, the numerical modelling technique became an effective tool for predicting permeability by incorporating the process variability of automated fiber placement. The precision of automated dry fibre placement can influence the distribution of gap size and tape overlap rate. By considering the AFP variability, the permeability would deviate from the target value based on the material design by a factor of 5. The study has revealed that the deviation of permeability was primarily due to gap size variation (60% contribution) and tape overlap rate (18% contribution). This evidence confirms that precise control of the gap size in automated fibre placement preforms is the most critical parameter to achieve the desired permeability. The modelling procedures developed herein can be employed to produce AFP preforms that exhibit a superior flow behavior and mechanical properties.

## 7.0 Acknowledgements

The authors would like to thank Dr. Sanjeev Rao for designing the permeability rig, Mr. Pradeep George and Mr. Jimmy Thomas at Khalifa University for their assistance in conducting the experiments. Also, thanks goes to Mr. Sam Hill, Mr. Sam Newton and Mr. Sebastien Greber from Solvay group for providing

valuable assistance in sourcing the dry tapes and preforms. The authors gratefully acknowledge Strata and Khalifa University for providing the financial support for this research project.

## 8.0 References

- [1] M. Yun, P. Simacek, S. Advani, Stochastic modeling of through the thickness permeability variation in a fabric and its effect on void formation during Vacuum Assisted Resin Transfer Molding. *Composites Science and Technology*, 149, 2017, pp100-107.
- [2] H. S. Sas, E. B. Wurtzel, P. Simacek and S. G. Advani, Effect of relative ply orientation on the through-thickness permeability of unidirectional fabrics, *Composites Science and Technology*, 96, 2014, pp116–121.
- [3] N. Kuentzer, P. Simacek, S. G. Advani and S. Walsh, Permeability characterization of dual scale fibrous porous media, *Composites Part A*, 37, 2006, pp2057–2068.
- [4] A. Endruweit, X. Zeng and A. C. Long, Multiscale modeling of combined deterministic and stochastic fabric non-uniformity for realistic resin injection simulation, *Advanced Manufacturing: Polymer & Composites Science*, 1, 2015, pp3–15.
- [5] H. Z. Jishi, R. Umer, W.J. Cantwell. Skin-core debonding in resin-infused sandwich structures. *Polymer Composites* 37 (10), 2016, pp2974-2981
- [6] K. Croft, L. Lessard, D. Pasini, M. Hojjati, J. Chen and A. Yousefpour, Experimental study of the effect of automated fiber placement induced defects on performance of composite laminates, *Composites Part A: Applied Science and Manufacturing*, 42, 2011, pp484–491.
- [7] D. H. J. A. Lukaszewicz, C. Ward and K. D. Potter, The engineering aspects of automated prepreg layup: History, present and future, *Composites Part B: Engineering*, 43, 2012, pp997–1009.
- [8] R. Umer, S. Rao, J. Zhou, Z. Guan, W.J. Cantwell. The low velocity impact response of nano modified composites manufactured using automated dry fibre placement. *Polymers & Polymer Composites* 24 (4), 2016, pp233.
- [9] <http://www.compositesworld.com/articles/resin-infused-ms-21-wings-and-wingbox> (online resource accessed on 02/07/2017).
- [10] <http://www.compositesworld.com/news/revolutionary-fuselage-concept-unveiled-by-mtorres> (online resource accessed on 02/07/2017).
- [11] N. Hassan, J. E. Thompson and R. C. Batra, A heat transfer analysis of the fiber placement composite manufacturing process, *Journal of Reinforced Plastics and Composites*, 24, 2005, pp869–888.
- [12] P. A. Kelly, R. Umer and S. Bickerton, Viscoelastic response of dry and wet fibrous materials during infusion processes, *Composites Part A: Applied Science and Manufacturing*, 37, 2006, pp868–873.
- [13] S. Bickerton, M. J. Buntain and A. A. Somashekar, The viscoelastic compression behavior of liquid composite molding preforms, *Composites Part A: Applied Science and Manufacturing*, 34, 2003, pp431–444.
- [14] K.A. Khan, R. Umer. Modeling the viscoelastic compaction response of 3D woven fabrics for liquid composite molding processes. *Journal of Reinforced Plastics and Composites*, 2017, DOI: 0731684417707263.
- [15] X. Xiao, A. Endruweit, X. Zeng, J. Hu and A. Long, Through-thickness permeability study of orthogonal and angle-interlock woven fabrics, *Journal of Materials Science*, 50, 2015, pp1257–1266.
- [16] H. Alhussein, R. Umer, S. Rao, E. Swery, S. Bickerton, W. Cantwell. Characterization of 3D woven reinforcements for liquid composite molding processes. *Journal of Materials Science*, 51, 2016, pp3277–3288.
- [17] C. D. Rudd, M. R. Turner, A. C. Long and V. Middleton, Tow placement studies for liquid composite moulding, *Composites Part A: Applied Science and Manufacturing*, 30, 1999, pp1105–1121.
- [18] S. Drapier, J. Monatte, O. Elbouazzaoui and P. Henrat, Characterization of transient through-thickness permeabilities of Non Crimp New Concept (NC2) multiaxial fabrics, *Composites Part A:*

- Applied Science and Manufacturing, 36, 2005, pp877–892.
- [19] M. Belhaj, M. Deleglise, S. Comas-Cardona, P. Figueiredo, Dry fiber automated placement of carbon fibrous preforms, *Composites Part B: Engineering*, 50, 2013, pp107–111.
- [20] O. Rimmel, D. Becker and P. Mitschang, Maximizing the out-of-plane-permeability of preforms manufactured by dry fiber placement, *Advanced Manufacturing: Polymer & Composites Science*, 2, 2016, pp93–102.
- [21] <http://texgen.sourceforge.net/index.php/Documentation>
- [22] B. R. Gebart, Permeability of unidirectional reinforcements for RTM, *Journal of Composite Materials*, 26, 1992, pp1100–1133.
- [23] B. Verleye, R. Croce, M. Giebel, M. Klitz, S. V. Lomov, G. Morren, H. Sol, I. Verpoest, D. Roose, Permeability of textile reinforcements: Simulation, influence of shear and validation, *Composites Science and Technology*, 68, 2008, pp2804–2810.
- [24] G. Chinga-Carrasco, O. Solheim, M. Lenes and Å. Larsen, A method for estimating the fibre length in fibre-PLA composites, *Journal of Microscopy*, 250, 2013, pp15–20.
- [25] E. N. Landis and D. T. Keane, X-ray microtomography, *Materials Characterization*, 61, 2010, pp1305–1316.
- [26] N. Vernet et al., Experimental determination of the permeability of engineering textiles: Benchmark II, *Composites Part A: Applied Science and Manufacturing*, 61, 2014, pp172–184.
- [27] M. Bodaghi, A. Vanaerschot, S.V. Lomov, N.C. Correia. On the variability of mesoscale permeability of a 2/2 twill carbon fabric induced by variability of the internal geometry. *Composites Part A: Applied Science and Manufacturing*, 101, pp.394-407.
- [28] X Zeng, A Endruweit, LP Brown, AC Long. Numerical prediction of in-plane permeability for multilayer woven fabrics with manufacture-induced deformation. *Composites Part A: Applied Science and Manufacturing*, 77, pp. 266-274.



## List of Figures

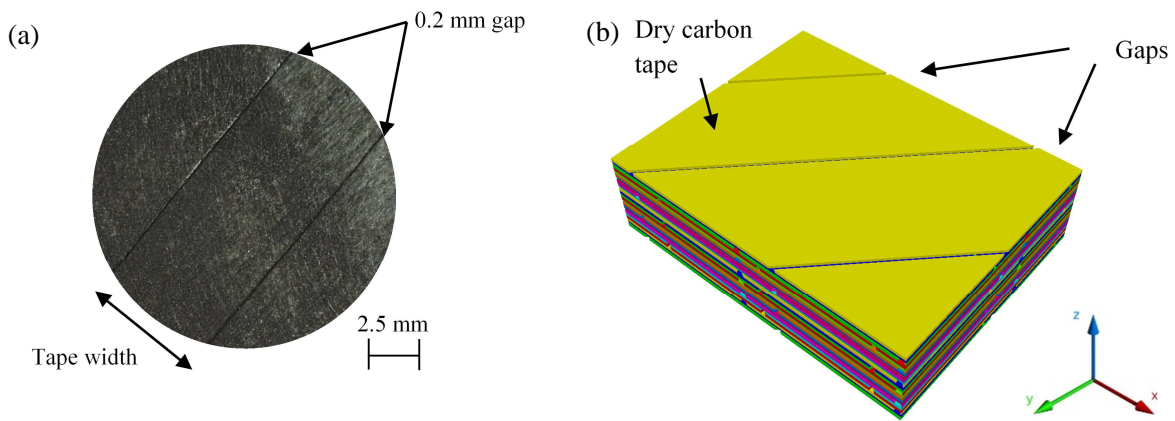
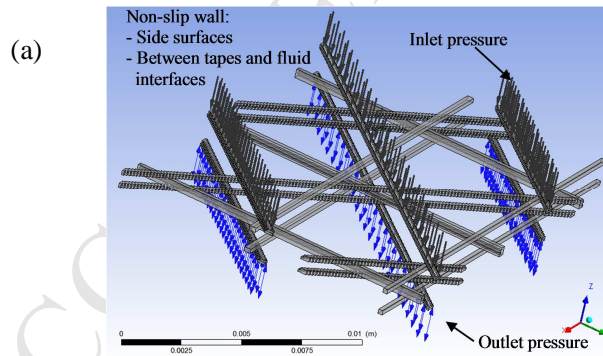


Figure 1: (a) Photograph of Preform A, a 6.35 mm wide dry fiber preform based on a gap size of 0.2 mm, (b) ANSYS model of Preform A, created by stacking 24 layers of unidirectional tape in a  $[+45/0/-45/90]_{3s}$  stacking sequence.



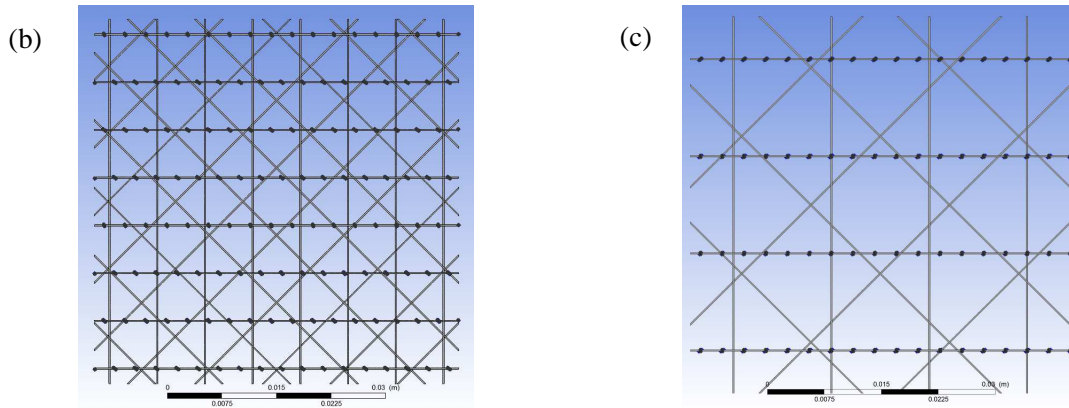


Figure 2: ANSYS model for through-thickness permeability predictions, (a) Summary of the boundary conditions used, (b) Top view of Preform A and, (c) Top view of Preform B.

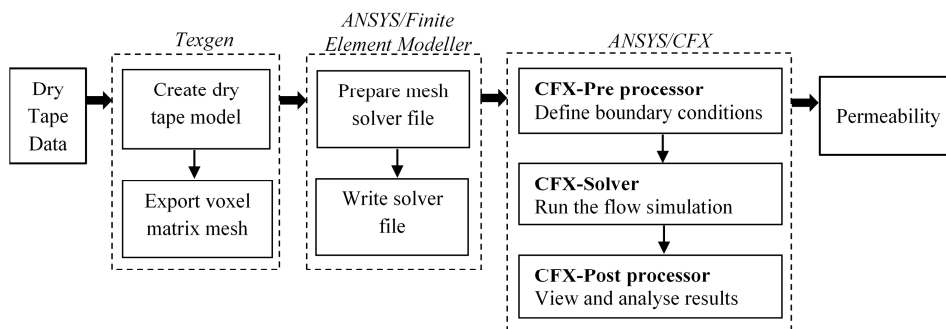
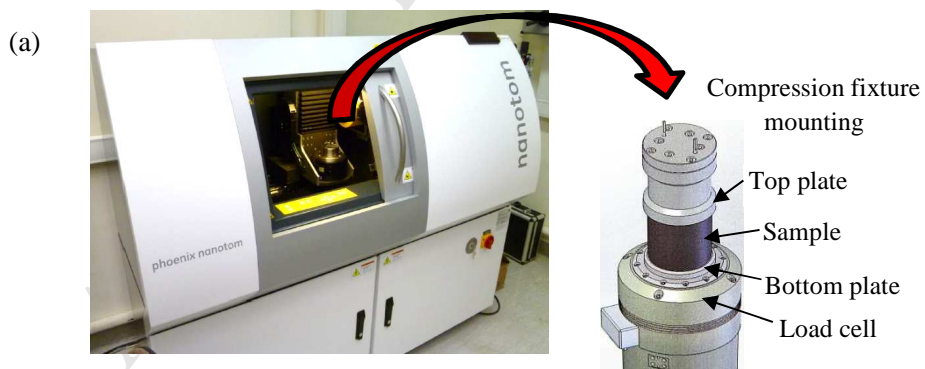


Figure 3: Flowchart for modelling the permeability characteristics of the dry fiber preform.



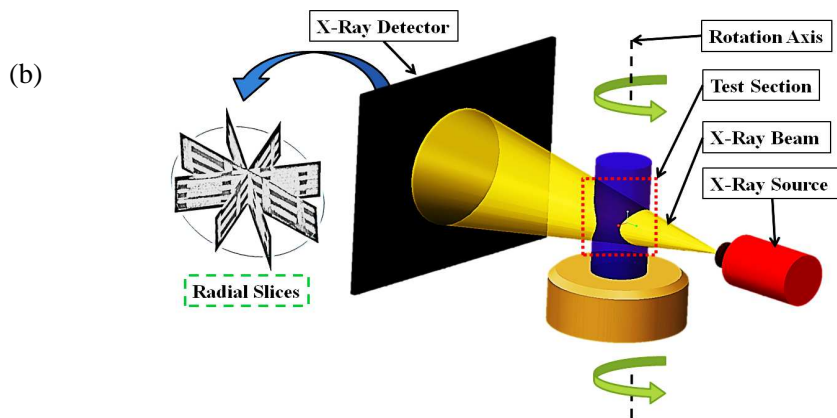


Figure 4: Experimental set-up of (a) the GE Phoenix Nanotom X-CT machine with compression fixture and, (b) an illustration of X-CT image acquisition process.

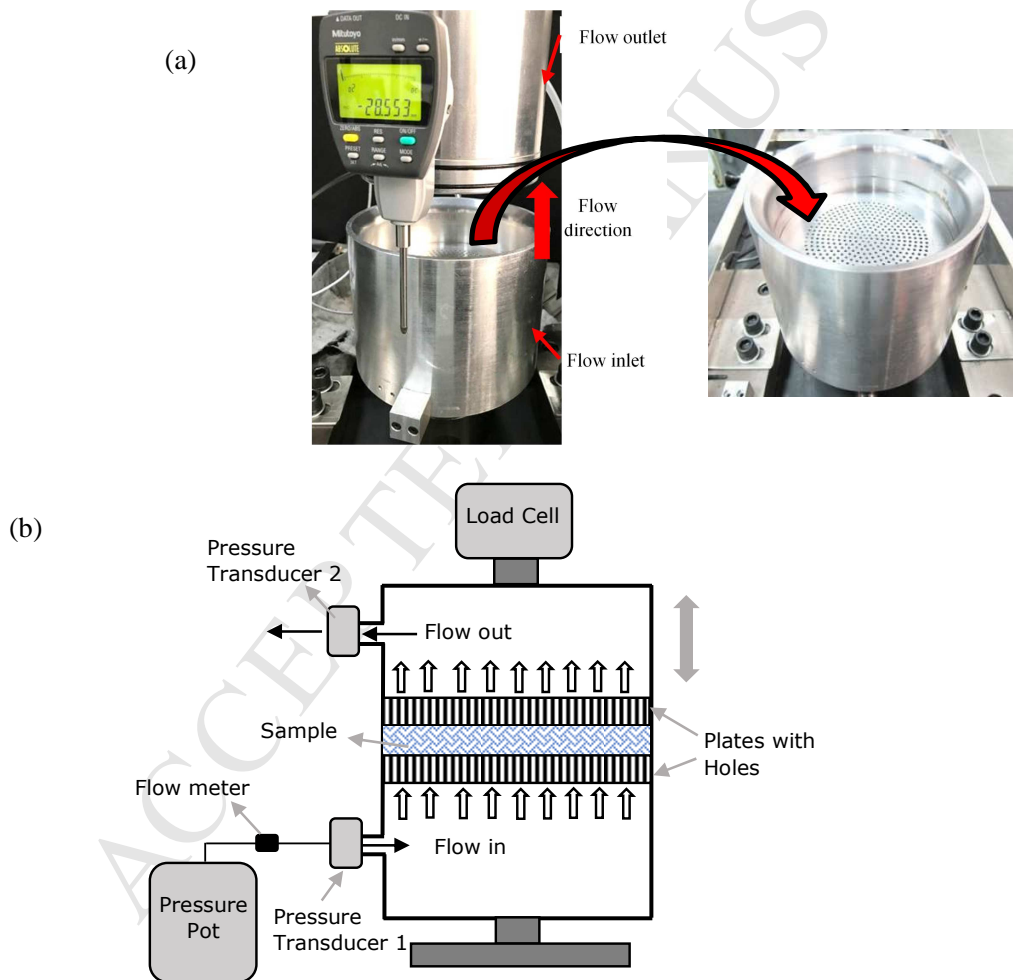


Figure 5: Photographs of (a) the fixture installed in a MTS machine with bottom half of the fixture showing plate with holes and, (b) a schematic of the through-thickness permeability experiment.

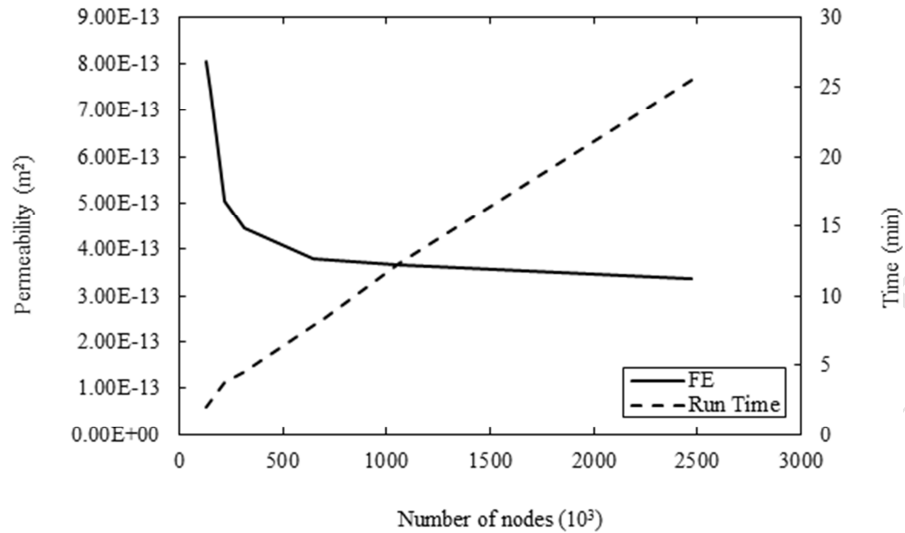


Figure 6: Mesh sensitivity study showing the number of nodes required for convergence of the CFD model for Preform A.

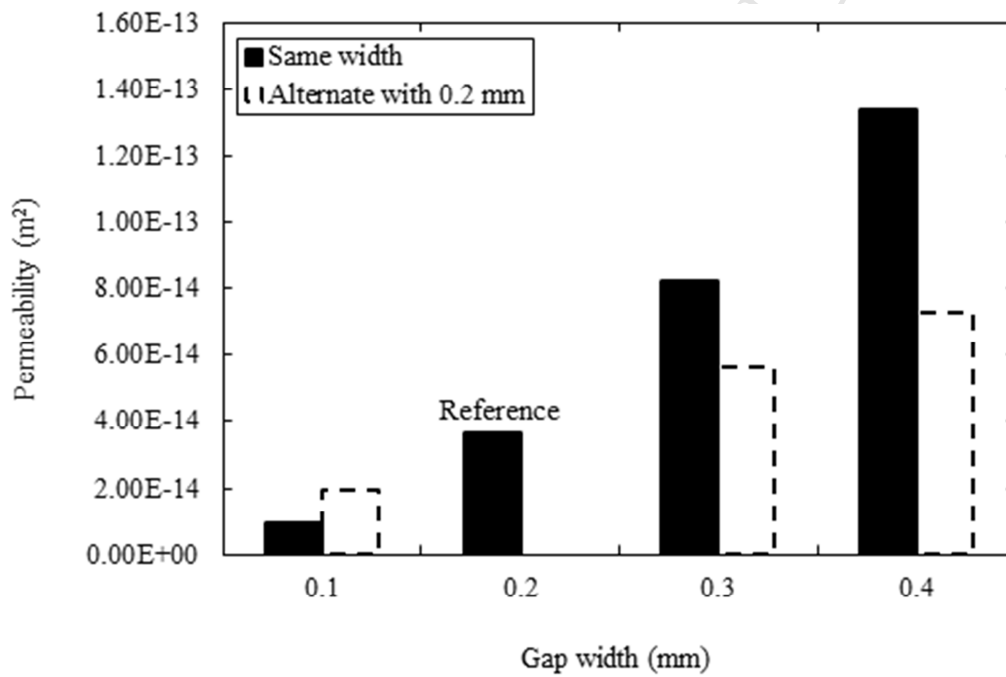


Figure 7: Parametric study to assess the effect of gap sizes on the permeability of Preform B.

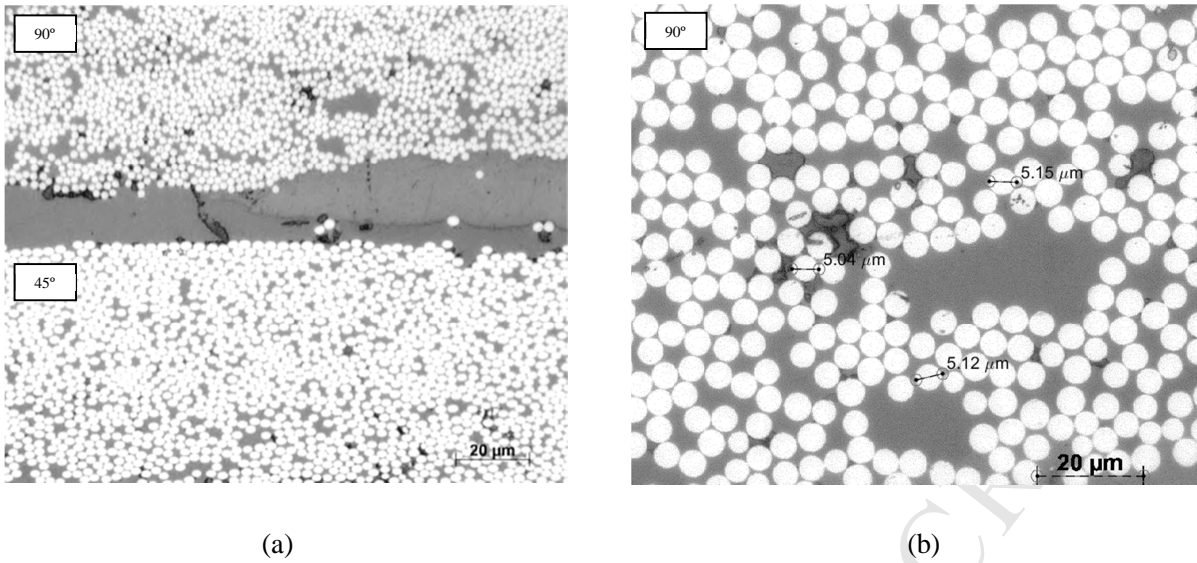


Figure 8: Cross-sections of Preform A after resin infusion, (a) close-up of two plies, and (b) close-up of individual fibers.

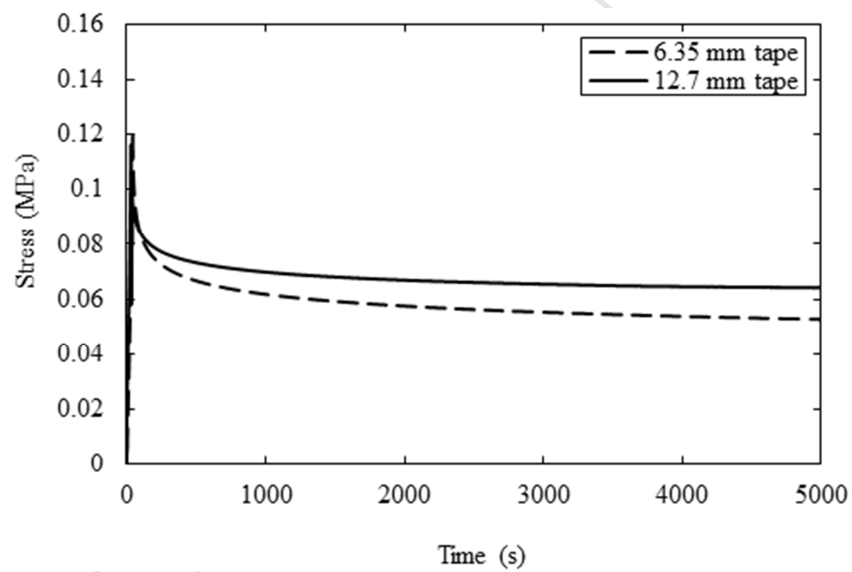
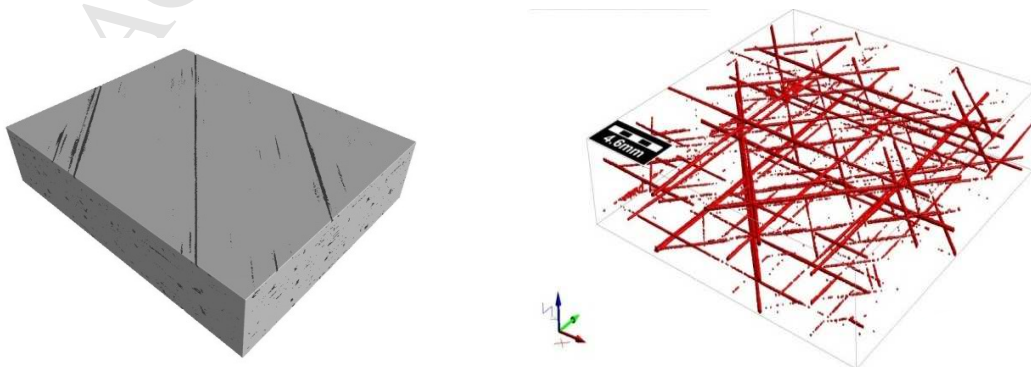


Figure 9: Stress relaxation plots during compression testing of Preform A and Preform B in the X-CT scanner.



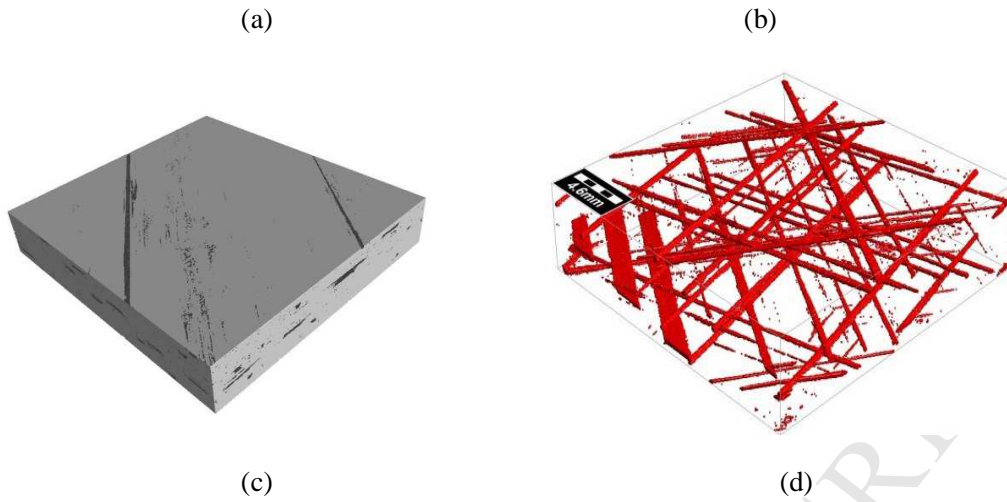


Figure 10: GeoDict analysis showing the distribution of pores in (a, b) Preform A, and (c, d) Preform B.

Ply Orientation	Preform A	Preform B
+45°		
0°		

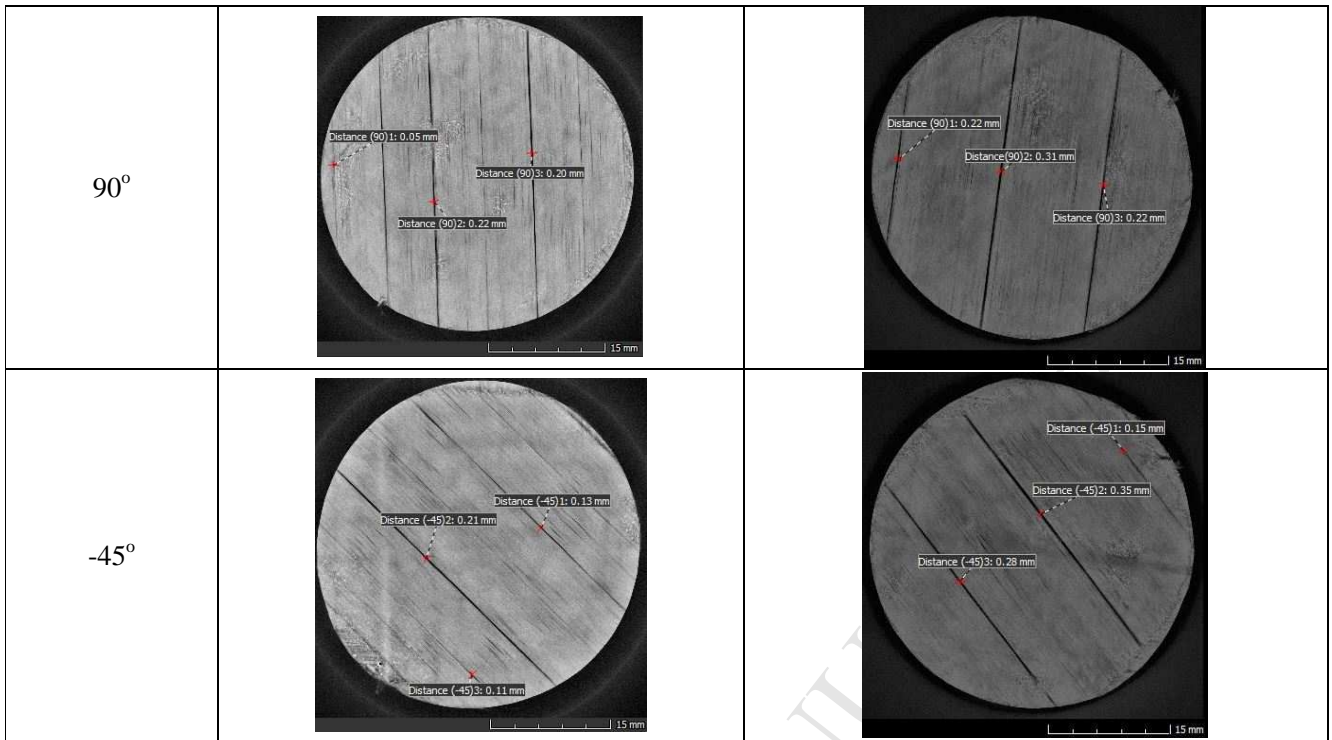
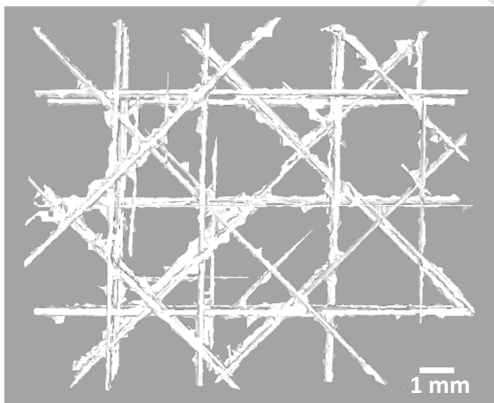
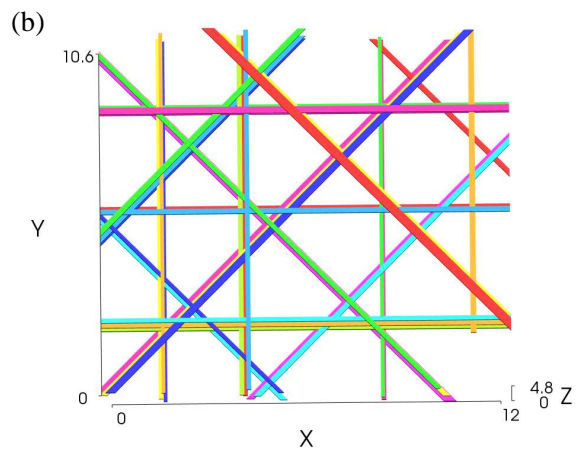


Figure 11: X-CT images taken under compression of Preform A and Preform B showing the variability of gap sizes between different plies.



(c)



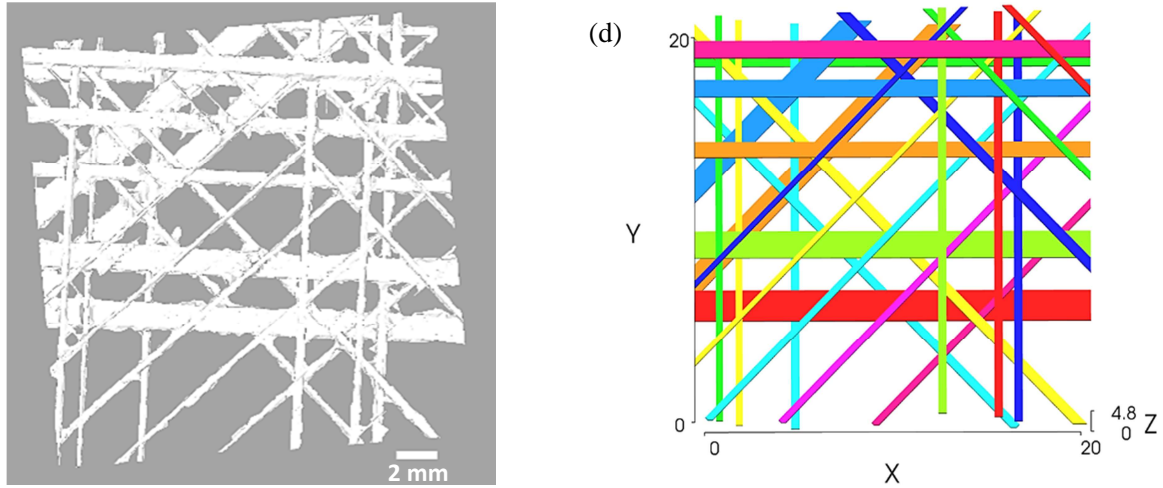


Figure 12: Through-thickness view of the stacked gaps in X-CT 3D scan and TexGen 3D model reconstructed from the X-CT scans for (a, b) Preform A, and (c, d) Preform B.

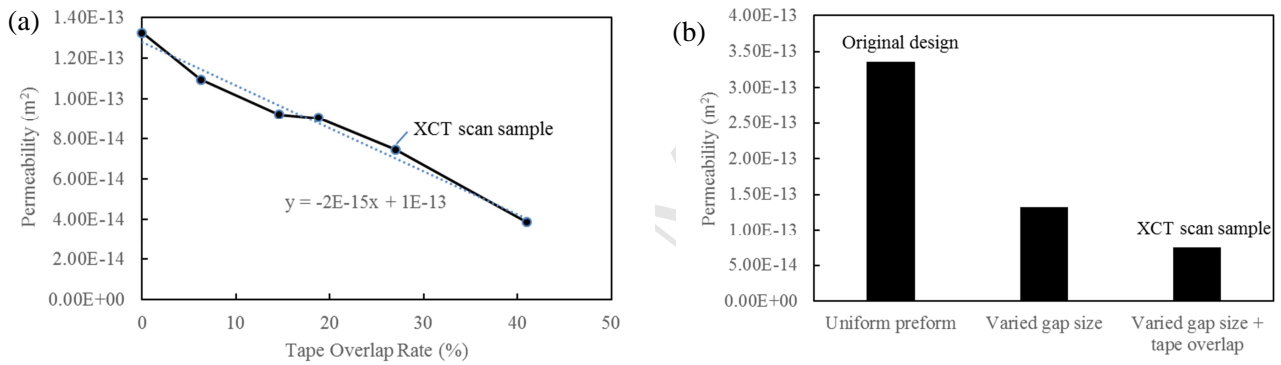


Figure 13: The effect of tape placement variability on through-thickness permeability based on the CFD prediction, (a) Parametric study of Tape Overlap Rate on permeability, (b) Combined effect of gap size and tape overlap.

## List of Tables

Table 1: Details of the mesh sensitivity analysis for the model of Preform A.

FE Model ID	Number of Nodes [ $10^3$ ]	Mesh size [mm]	Permeability [ $m^2$ ]	CPU time [minutes]
q22-12	128	0.12	$8.05 \times 10^{-13}$	2.04
q22-10	156	0.10	$7.39 \times 10^{-13}$	2.43



q22-08	221	0.08	$5.06 \times 10^{-13}$	3.71
q22-07	317	0.07	$4.45 \times 10^{-13}$	4.49
q22-06	606	0.06	$4.12 \times 10^{-13}$	6.82
q22-05	648	0.05	$3.80 \times 10^{-13}$	7.87
q22-04	1,057	0.04	$3.67 \times 10^{-13}$	12.34
q22-03	2,473	0.03	$3.36 \times 10^{-13}$	25.47

Table 2: Gap and permeability values for the dry tape preforms, simulations vs. experiments.

Preform sample	Tape width (mm)	% Gaps		Permeability [ $m^2$ ]					%Error (Exp vs. Design)	%Error (Exp vs. X-CT)
		Design	X-CT	Experiment			CFD (Design)	CFD (X-CT)		
				Test	Average	Unpaired t-test p-value				
Preform A	6.35	3.1	1.5	$8.51 \times 10^{-14}$	$8.31 \times 10^{-14}$	0.07	$3.87 \times 10^{-13}$	$7.47 \times 10^{-14}$	366	-10
				$7.66 \times 10^{-14}$						
				$8.75 \times 10^{-14}$						
Preform B	12.7	1.5	3.5	$2.52 \times 10^{-13}$	$1.85 \times 10^{-13}$	0.07	$3.65 \times 10^{-14}$	$2.04 \times 10^{-13}$	-80	10
				$1.09 \times 10^{-13}$						
				$1.94 \times 10^{-13}$						

Table 3: Details of the CFD parametric study on the effect of gap size on the permeability of Preform B.

FE Model ID	Tape width [mm]	% Gaps	Gap width [mm]	Alternate gap width [mm]	Permeability [ $m^2$ ]
h50-01	12.7	0.8	0.1	-	$9.61 \times 10^{-15}$
h50-02	12.7	1.5	0.2	-	$3.65 \times 10^{-14}$
h50-03	12.7	2.3	0.3	-	$8.24 \times 10^{-14}$

h50-04	12.7	3.0	0.4	-	$1.34 \times 10^{-13}$
h50-21	12.7	1.1	0.1	0.2	$1.95 \times 10^{-14}$
h50-23	12.7	1.9	0.3	0.2	$5.62 \times 10^{-14}$
h50-24	12.7	2.3	0.4	0.2	$7.31 \times 10^{-14}$